

Chemical Composition of Micrometer-Sized Filaments in an Aragonite Host by a Miniature Laser Ablation/Ionization Mass Spectrometer

Marek Tulej,¹ Anna Neubeck,² Magnus Ivarsson,³ Andreas Riedo,¹ Maike B. Neuland,¹ Stefan Meyer,¹ and Peter Wurz¹

Abstract

Detection of extraterrestrial life is an ongoing goal in space exploration, and there is a need for advanced instruments and methods for the detection of signatures of life based on chemical and isotopic composition. Here, we present the first investigation of chemical composition of putative microfossils in natural samples using a miniature laser ablation/ionization time-of-flight mass spectrometer (LMS). The studies were conducted with high lateral ($\sim 15\ \mu\text{m}$) and vertical ($\sim 20\text{--}200\ \text{nm}$) resolution. The primary aim of the study was to investigate the instrument performance on micrometer-sized samples both in terms of isotope abundance and element composition. The following objectives had to be achieved: (1) Consider the detection and calculation of single stable isotope ratios in natural rock samples with techniques compatible with their employment of space instrumentation for biomarker detection in future planetary missions. (2) Achieve a highly accurate chemical compositional map of rock samples with embedded structures at the micrometer scale in which the rock matrix is easily distinguished from the micrometer structures. Our results indicate that chemical mapping of strongly heterogeneous rock samples can be obtained with a high accuracy, whereas the requirements for isotope ratios need to be improved to reach sufficiently large signal-to-noise ratio (SNR). Key Words: Biogenicity—Biomarkers—Biosignatures—Filaments—Fossilization. *Astrobiology* 15, 669–682.

1. Introduction

IN *SITU* DETECTION of life signatures in extraterrestrial geological material is highly prioritized on current and upcoming missions such as ExoMars or Mars 2020. Possible traces of life to search for would be geochemical signatures such as mineralogy indicative of habitable environments or element composition and isotopic fractionation indicative of biology or metabolic processes (Chela-Flores and Kumar 2008; Chela-Flores and Seckbach 2011; Chela-Flores *et al.*, 2015). Other signs of life would be molecular or body fossils of microorganisms (Westall *et al.*, 2001; Leshin *et al.*, 2013). Separately, such signals are usually not sufficient to prove the presence of past life, but found together they can be used to argue biogenicity (Summons *et al.*, 2011). Fossilized microorganisms could, at optimal conditions, contain morphological, molecular, and geochemical signatures concentrated in a defined micrometer-sized structure and are thus suitable

for such investigations. However, analysis of microfossils and subsequently establishing their biogenicity are not an easy task, not even in terrestrial samples (Brasier *et al.*, 2005). Detection and characterization of possible microbial remains in extraterrestrial samples are thus a challenge for the whole astrobiological community, and there is an urgent need for the development of new and more sensitive instrumentation capable of *in situ* detection of molecular and elemental biosignatures on other planetary bodies.

Current space instrumentation includes sophisticated sampling instruments that have the capacity to deliver the physical and chemical composition of planetary surfaces and subsurfaces (Grotzinger *et al.*, 2012). Further development of sensitive, more specific space instrumentation for context investigation is of considerable interest and is an ongoing process (Parnell *et al.*, 2007; Chela-Flores, 2010, 2012). The instruments for the investigation of planetary context are particularly interesting. They would allow the

¹Physics Institute, Space Research and Planetary Sciences, University of Bern, Bern, Switzerland.

²Department of Geological Sciences, Stockholm University, Stockholm, Sweden.

³Department of Palaeobiology and Nordic Centre for Earth Evolution (NordCEE), Swedish Museum of Natural History, Stockholm, Sweden.

search for, and *in situ* detection of, fossilized microorganisms on rocks or in minerals. On Mars, there could be various microniches where fossilized microorganisms could be searched for. Microorganisms are favored by the presence of liquid water, and such environments are usually characterized by high rates of mineralization, which in turn is favorable for microbial entrapment, preservation, and subsequent fossilization. Hydrothermal environments on Earth are known for their abundant microbial presence coupled with frequent and rapid mineralization of, for example, silica, carbonates, or sulfates, in which microorganisms are trapped (Reysenbach and Cady, 2001). Hydrothermal activity has been present throughout Mars' history up until recently (Farmer, 2001). Rovers and orbiters have detected mineral suites on the surface of Mars that are indicative of hydrothermal activity and represent perfect candidate environments where microbial life could have existed and been preserved (Bishop *et al.*, 2008; Mustard *et al.*, 2008; Squyres *et al.*, 2008). Another type of mineralization that has been found on the surface of Mars is that of the evaporates. Such mineralization represents hypersaline lakes, in which microorganisms are known to thrive and are easily trapped by the formation of salt crystals. Polar ice is also a mineral that represents a habitable environment characterized by rapid mineralization. However, microbes can also exist on rock substrates in extremely dry areas such as deserts. Rock varnish is a Mn- and Fe-rich mineral crust that forms on rocks in dry areas such as Antarctica and is the result of microbial activity (Gorbushina, 2003). In these mineral crusts, the remains of the active microorganisms are preserved and easily detectable. Rock varnish could form on Mars and should be targeted on upcoming missions (Gorbushina *et al.*, 2002).

The hostile surface conditions on Mars, including radiation and temperature fluctuations, imply that the subsurface is a more plausible environment where microbes could survive and, thus, be preserved over geological time. Fossilized microbial communities in mafic rocks have been found in both continental and marine environments on Earth and could be considered as analogues to potential extraterrestrial communities basically because mafic rocks are the dominating rock type on other terrestrial planets.

In the search for biosignatures, which could be efficiently applied for *in situ* investigations on the surfaces of other planets, the knowledge of key biorelevant elements and their isotopic composition, which are affected by biological fractionation, are of foremost interest (Chela-Flores and Kumar, 2008; Chela-Flores, 2010; Chela-Flores and Seckbach, 2011). Typically, only large and complex laboratory instruments are used to obtain quantitative elemental and isotopic composition of micrometer-sized objects (Zinner *et al.*, 2011; Ireland, 2013). Detection of elements and their isotopes to differentiate between biotic and abiotic materials can be investigated by currently available miniature mass spectrometric instruments (Brinckerhoff *et al.*, 2000; Rohner *et al.*, 2003, 2004; Managadze *et al.*, 2010). Performance studies of a miniature laser ablation/ionization time-of-flight mass spectrometer (LMS) system developed for space research in our group have been reported in several recent publications (Riedo *et al.*, 2010, 2013a, 2013b; Tulej *et al.*, 2011, 2014; Neuland *et al.*, 2014; Grimaudo *et al.*, 2015). Laser ablation/ionization mass spectrometry allows for highly sensitive detection of

almost all elements and isotopes with their concentrations down to tens of parts per billion at significantly better than unit mass resolution. High spatial resolution of the surface analysis is achieved by focusing the laser to a spot of 10–20 μm , allowing for chemical surface mapping and depth profiling (Neuland *et al.*, 2014; Grimaudo *et al.*, 2015).

In the present study, we investigated for the first time micrometer-sized filamentous structures embedded in carbonate veins in harzburgite by microscopic imaging and laser ablation mass spectrometry. We present the chemical analysis of the microstructures and discuss the implications of the chemical analysis as well as a possible biological origin. Based on this work, we are confident that similar studies can be conducted *in situ* on planetary surfaces and will be essential in searches for past life.

2. Materials and Methods

2.1. Sample preparation

The sample (1271B 4R1 23–26 cm) used in the current study was acquired from the slow-spreading Mid-Atlantic Ridge during ODP Leg 209 and collected from a depth of 26.9 m below the seafloor (Bach *et al.*, 2011). The sample contains aragonite veins hosted in serpentinized harzburgite. The age of the aragonite is >54,900 years since it is radiocarbon-dead, but not more than 1 million years since that is the approximate time when the basement exhumed (Bach *et al.*, 2011).

The sample was prepared as a polished thin section ($\sim 30 \mu\text{m}$ in thickness). Mineral phases and putative fossilized microorganisms were localized by an optical microscope and an environmental scanning electron microscope (ESEM) coupled with an energy-dispersive spectrometer (EDS) on an FEI QUANTA FEG 650 (Oxford Instruments, UK). For the analysis by EDS, an Oxford T-Max 80 detector was used. The sample was not coated during ESEM/EDS analyses. To minimize surficial charging effects, the sample was kept at low-vacuum conditions, and the acceleration voltage was kept at 20 or 15 kV depending on the nature of the sample. The instrument was calibrated with a cobalt standard. Peak and element analyses were performed with INCA Suite 4.11 software.

2.2. Laser mass spectrometry

2.2.1. Sample preparation for mass spectrometric analysis. For the mass spectrometric investigation, a polished thin section of the sample was mounted on the sample holder and imaged with a laboratory microscope to identify the regions with potential fossilized material (Fig. 1A). After selection of rectangular areas on the sample surface (Fig. 1B), the *x-y* coordinates were introduced and transformed to the coordinate system of an *x-y-z* translational stage on which the sample was mounted (Riedo, 2014). The sample was then placed into the measurement vacuum chamber at the measurement location (Riedo *et al.*, 2013a, 2013c). Two different surface areas (M1 and M2) were investigated (Fig. 1A). Figure 1B displays a microscope image of the surface area selected for the mass spectrometric analysis in the first campaign (M1). A similar rectangular area was investigated a few months later from the second surface location (M2, Fig. 1A).

2.2.2. Laser ablation/ionization mass spectrometry. The mass spectrometric investigation was conducted by a miniature LMS designed for *in situ* space research (Rohner

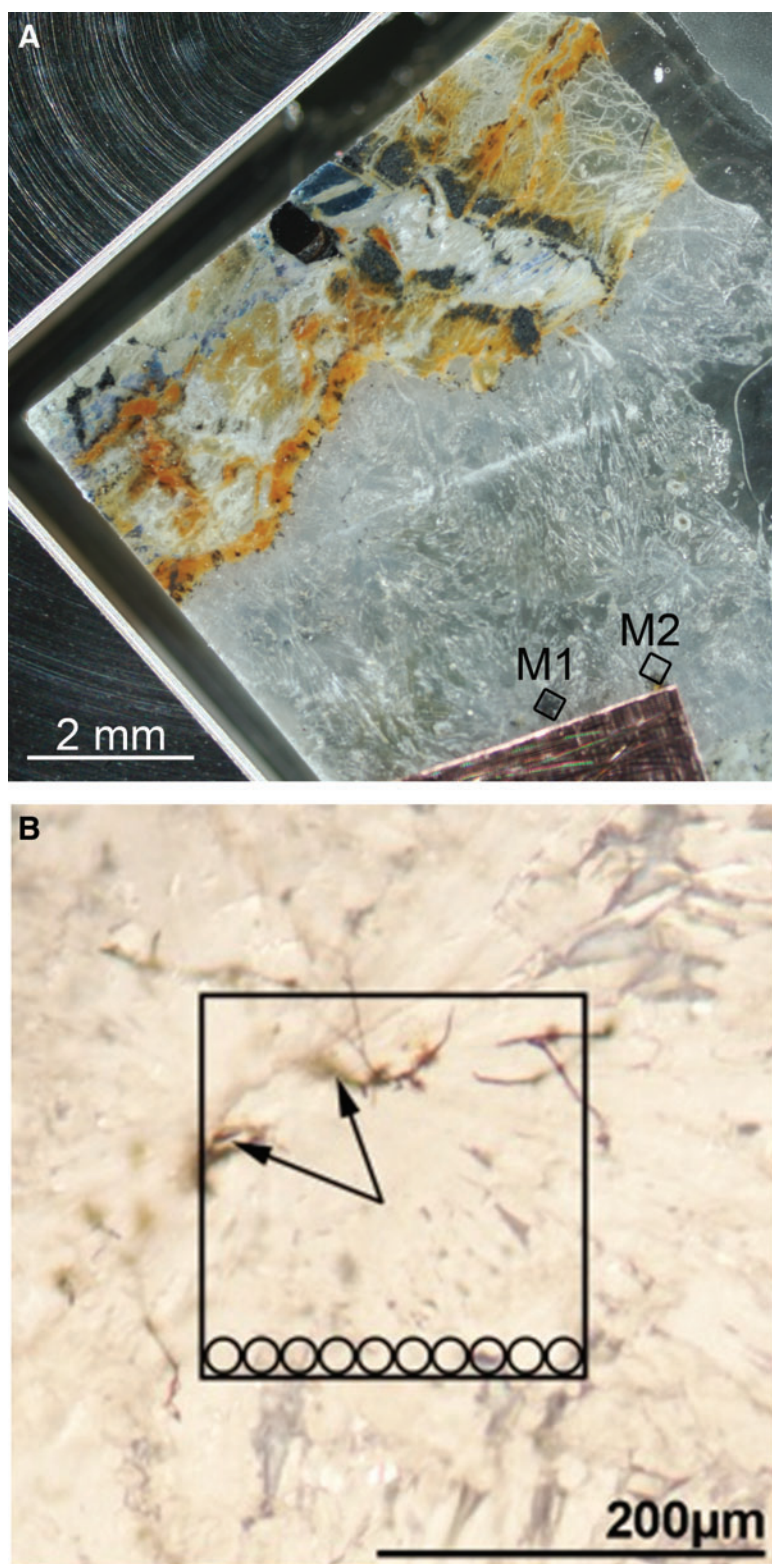


FIG. 1. Images of the investigated sample. (A) Image of the thin section of the sample placed on the sample holder, including the locations of the investigated areas M1 and M2 (each $200 \times 200 \mu\text{m}$). (B) Detail of the sample surface used for systematic high-resolution chemical mapping by mass spectrometry during the first campaign (M1). The studies are conducted within a rectangular area containing filamentous microstructures. The circles inserted in the picture are scaled to the laser spot size. (Color graphics available at www.liebertonline.com/ast)

et al., 2003). The instrument combines laser ablation/ionization ion source with a reflectron time-of-flight mass analyzer. The details of the technical realization and principles of operation of LMS are described in previous publications (Riedo *et al.*, 2013a, 2013b, 2013c). In the current investigations, a focused fs-laser radiation ($\tau \sim 190$ fs,

$\lambda = 775$ nm, laser pulse repetition rate of 1 kHz) was used to ablate, atomize, and ionize sample material. Laser pulse energy, laser pulse repetition rate, and the number of applied laser pulses were fully computer controlled by the LMS operating system (Riedo *et al.*, 2013a, 2013c; Riedo, 2014). The laser focus (a spot of about $15 \mu\text{m}$ in diameter) was

arranged on a sample surface placed on x - y - z micro translation stage, about 1 mm away from the entrance to the LMS ion-optical system.

2.2.3. Measurement procedure. Mass spectrometric measurements were conducted on rectangular areas (M1 and M2, each $200 \times 200 \mu\text{m}^2$, with and without filamentous microstructures) (see Fig. 1). Because no microscope-camera system is currently installed in the instrumental setup to visualize sample surface *on line* the selected surface areas were investigated stepwise every $20 \mu\text{m}$ (raster of 10×10 surface locations) corresponding to 100 single investigated surface locations (Fig. 1). The measurement campaigns were realized in a sequential measurement procedure [by homemade software for the control of the acquisition system, micro translational stages, and laser system (Riedo, 2014; Tulej *et al.*, 2014)], including, first, the positioning of the micro translational stage to the desired surface location and the subsequent analysis by laser mass spectrometry. The calibration of the x - y - z stages with the x - y coordinates of the sample could be set with an accuracy of about $\pm 10 \mu\text{m}$. These studies yield chemical surface mapping with high lateral resolution.

The instrument also allows high-resolution chemical depth profiling (Grimaudo *et al.*, 2015). In the latter studies, the sample can be analyzed layer by layer with a depth resolution down to subnanometer per single laser shot. Further details of the technical realization and the principle of operation of LMS can be found in recent publications (Riedo *et al.*, 2013a, 2013b, 2013c).

A laser irradiance of $\sim 5.5 \text{ TW/cm}^2$ ($\sim 2 \mu\text{J/laser shot}$) was applied at the sample surface, which typically is sufficiently large to support stoichiometric ion production of metal-containing samples (Riedo *et al.*, 2013c; Grimaudo *et al.*, 2015). From each investigated surface location, 40,000 single laser shot mass spectra were recorded in 20 packets of 2000 summed individual waveforms each during the first campaign (M1). A similar campaign (M2) was conducted on another surface area of similar size a few months later, and 60,000 single laser shot mass spectra were recorded in 300 packets of 200 summed individual waveforms. Hence, for campaign M1 there are 20 and for campaign M2 there are 300 mass spectra per measurement location. The latter studies allow a 15 times increase of depth profiling resolution because the chemical information is obtained from thinner ablation layers and therefore also more accurate determination of the filament location in the aragonite host. Because, in the present study, the identification of the elements contained in the filaments was relevant, the quantitative ablation depth analysis was not conducted. Thus, the measurements yield only qualitative information on the ablation depth. Nevertheless, based on our current performance investigation on the chemical depth profiling, the vertical resolution of the ablation studies of filaments is expected to be in the range of 20–200 nm (Grimaudo *et al.*, 2015). For the chemical analysis of the filaments, only the mass spectra with the specific elements contained in filaments are considered. Because the laser ablation ion source was operated under the same conditions in both campaigns (similar laser spot diameter and applied laser fluence), ion rates that were also produced during the ablation were expected to be similar. By plotting the mass peak intensities of the elements contained only in the fila-

ments against the spectrum number (location, depth), the element contribution from the filaments can be well isolated from that of the aragonite host alone.

2.2.4. Data analysis. Two sets of mass spectra were recorded on two surface locations, each of $200 \times 200 \mu\text{m}^2$ size, in two campaigns, M1 and M2, respectively. The mass spectrometric analyses yielded the atomic abundance of elements determined in the sample. The combined error of the mass peak integration, background and noise, and statistics is typically lower than a few percent, and scaling of the signals by RSC is not applied (Riedo *et al.*, 2013c). Isotope abundance values for selected elements are calculated according to established procedures and can be presented with the usual delta notation:

$$\delta(v_{\text{heavy}}) = [(R_x/R_s) - 1] * 1000$$

where R denotes the isotope ratio of the heavy to light isotope (e.g., $^{34}\text{S}/^{32}\text{S}$), and R_x and R_s are the ratios in the sample and in the standard, respectively.

3. Results

3.1. Carbonate veins and filamentous microstructures: microscope observations

The investigations were conducted on dark filamentous micrometer-structures at the interface between the aragonite and the harzburgite host rock. The filaments have a uniform diameter of about 2–5 μm and range in length from about 20 to more than 100 μm (see Fig. 1). The veins are 5–10 mm in diameter, and the filaments are anchored to the vein walls of the host rock or occur closely associated with the vein walls embedded in the aragonite. They are quasi linear, frequently branched, and in some cases show repeated partitioning by perpendicular cross-walls similar to septa. We refer to them as micrometer-structures (filaments) that bear resemblance to known fossilized microorganisms.

3.2. Identification of the aragonite matrix and filament regions by mass spectrometry

The locations of filaments were found by plotting the signals of selected isotopes of specific elements contained just in the filaments against the recorded file numbers. The file number defines, in addition to lateral location of the filament, the number of the ablated layer at the measurement location. Figure 2 shows the locations of filaments identified by this method for those recorded mass spectra that contain B and S mass peaks (see also Fig. 3). Concentrations of B and S are observed to be increasingly high in the filaments, and they are practically undetectable in the aragonite host matrix. The peaks displayed in Fig. 2 have different heights and widths. While the height of the peak is related to the concentration of the element within the analyzed surface ablation layer, the peak width (a number of ablation layers) is related to vertical extension of the filamentous structure at a particular location. Thus, the search method allows a sensitive identification of filaments in the aragonite matrix volume within the instrumental sensitivity with a high spatial (lateral and vertical) resolution.

Analyses of the mass spectra showed that some of the filaments were detected directly at the surface (M1: file

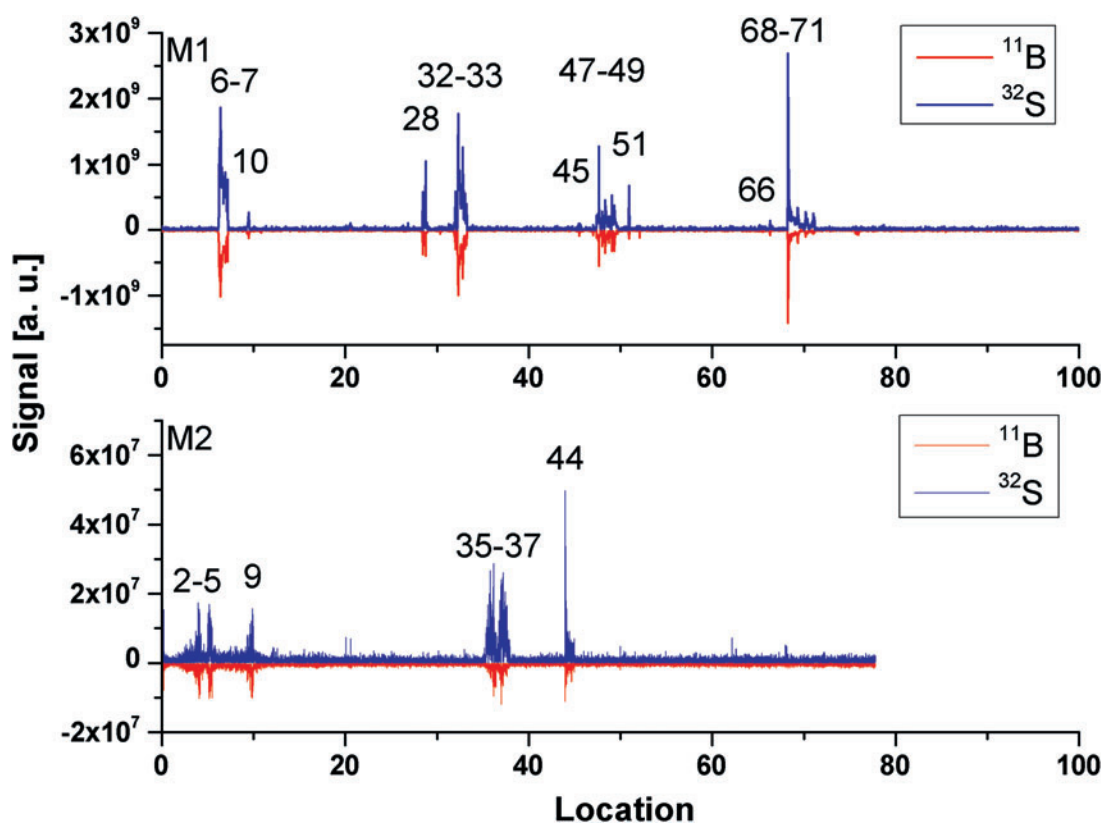
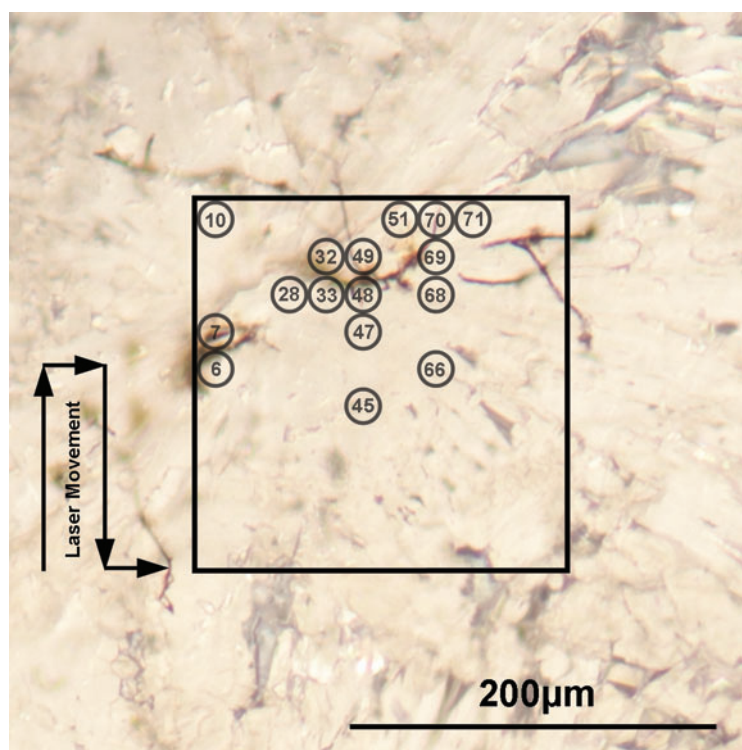


FIG. 2. Signals of the isotopes ^{11}B and ^{32}S are identified at several locations on the sample surface and subsurface. Peak shape in the graph reflects the variation of the detected signal with the progress of the ablation of the surface at a particular location. Compare also the correlation between the measurement locations (M1, upper panel) with the locations on the image recorded by a microscope-camera (Fig. 3). The signal of ^{11}B is reverted here. (Color graphics available at www.liebertonline.com/ast)

FIG. 3. The filament locations identified on the surface area during the first measurement campaign (M1). The circles with centered numbers in the figure show the locations at which the mass spectra characteristic for filaments were recorded by mass spectrometry (see also Fig. 2). The location of the circles is given with the accuracy of about $\pm 10 \mu\text{m}$. (Color graphics available at www.liebertonline.com/ast)



numbers 6, 33, 47–49, 68–71; M2: 35–37, 44) and others at the subsurface, after ablating some layers of the aragonite matrix (*e.g.*, M1: 10, 28, 32, 45, 51, 66; M2: 2, 3, 9, 35). The locations of the filaments identified by mass spectrometry are consistent with the filamentous microstructures observed in Fig. 3. At locations 10, 28, 45, 51, and 66, the microscope observation does not provide evidence on the filamentous structure, which indicates that detected features may be smaller or sufficiently diffuse to be observed readily. The lateral mapping and depth profile analysis helps to differentiate between the measurement of aragonite matrix and filaments. Note that the lateral resolution of the analysis is limited by the laser ablation spot size. For the filament sizes smaller than 15 μm , the elements contained in the aragonite matrix will contribute to the mass spectrum as well and render the quantitative chemical analysis less certain.

3.2.1. Chemical composition of aragonite host. The optical inspection of the sample surface by microscope showed that most of the measurements performed on the two selected surface areas yielded the mass spectra of the aragonite mineral (CaCO_3), which hosts the filaments. Mass spectra recorded in the low gain (LG) and high gain (HG) channels of the aragonite matrix are shown in Fig. 4. The LG spectra deliver the measurement of elements with concentrations down to a few hundreds of parts per million, whereas the HG spectra yield detection of elements with

concentrations down to a few tenths of parts per billion (Riedo *et al.*, 2013a). In the measurements conducted here, the LG mass spectrum shows the measurement of the major elements: H, K, Na, Ca, C, O, and Mg. Most aragonite minerals are nearly pure calcium carbonate (CaCO_3), though our measurements show, in addition to Ca, C, and O, the elements H, Na, K, and Mg. The atomic fractions of the (C, O, Ca) elements are observed to be not exactly stoichiometric (Table 1) with large deficiency of O element. Nevertheless, the mass spectrometric analysis delivers only the detection of S and Cl elements at the trace level (see Fig. 4). The identification of these elements in the aragonite matrix has to be considered as tentative because the presence of sufficiently diluted filamentous structures cannot be excluded in the investigated area. Isobaric interferences due to observation of clusters and molecules limit the detection sensitivity for other possible trace elements.

The example of the chemical depth profiling of the aragonite matrix prepared across 300 ablated layers (60,000 laser shots) at location 60 (M2) is presented in Fig. 5. The graphs display the signal variation of several elements with the ablation depth, given as the ablated layer number. The ablated layer is defined here as the surface thickness that was ablated by 200 laser shots. The signal variation observed in this study is similar to that typically observed in ablation studies of homogeneous material. After initial rise for the first few ablation layers (crater building, removal of the first uppermost

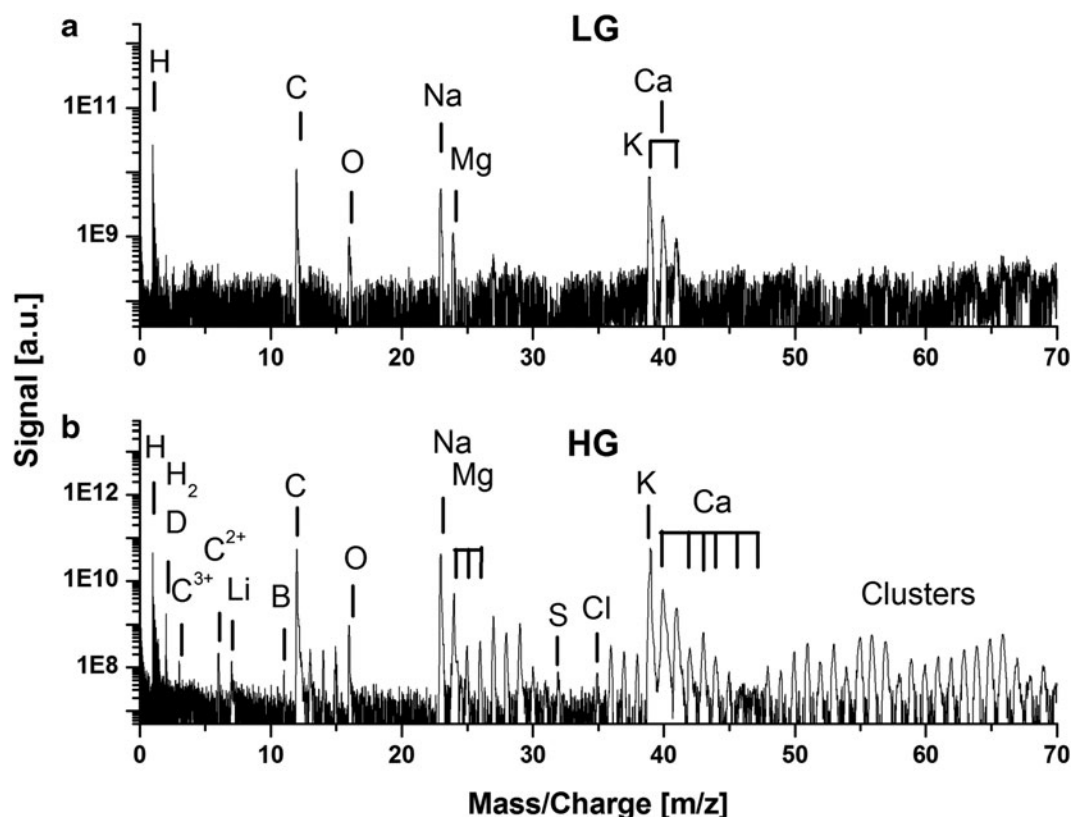


FIG. 4. Mass spectrum of the aragonite mineral (M1). (a) The low gain (LG) spectrum (upper panel) yields the detection of the major elements with the atomic fractions down to hundreds of parts per million. (b) The high gain (HG) spectrum is recorded simultaneously and shows, in addition, the mass peaks of trace elements, *e.g.*, S and Cl. Also several mass peaks of carbon clusters are identified in the mass range 24–27, 36–46, 48–70. Note that in the HG channel the most intense mass peaks of C, Na, and K are measured at the detector saturation (Riedo *et al.*, 2013a).

TABLE 1. ATOMIC FRACTIONS OF MAIN ELEMENTS MEASURED IN THE SELECTED FILAMENTS AND OF ALL FILAMENTS INVESTIGATED IN BOTH M1 AND M2 CAMPAIGNS, RESPECTIVELY

	<i>Loc_33</i>	<i>Loc_48</i>	<i>All_M1</i>	<i>Loc_36</i>	<i>Loc_44</i>	<i>All_M2</i>	<i>Aragonite matrix</i>
C	2.31 (0.04)	2.06 (0.07)	4.93 (0.08)	2.27 (0.07)	2.17 (0.12)	3.07 (0.02)	15.00 (0.7)
O	3.18 (0.12)	8.18 (0.115)	4.00 (0.10)	6.75 (0.15)	6.83 (0.11)	7.89 (0.01)	3.14 (0.04)
Na	20.43 (0.19)	22.8 (0.22)	23.77 (0.04)	29.25 (0.22)	20.84 (0.29)	18.94 (0.29)	27.14 (0.03)
Mg	8.30 (0.07)	11.70 (0.09)	8.03 (0.02)	9.86 (0.09)	11.37 (0.13)	4.59 (0.15)	2.41 (0.02)
K	23.19 (0.17)	20.19 (0.19)	24.18 (0.07)	29.87 (0.19)	20.16 (0.29)	22.16 (0.29)	40.58 (0.1)
Ca	9.18 (0.08)	15.73 (0.05)	14.93 (0.02)	9.39 (0.05)	11.07 (0.06)	6.23 (0.06)	10.72 (0.01)
Other	33.41	19.34	20.16	12.61	27.56	19.43	(Li, S, Cl) < 100 ppm

The atomic fractions of the elements determined for aragonite matrix are given in the last column.

atomic layers of the sample surface), overall signals rapidly decrease and begin to stabilize for the rest of the ablation progress. The ion rates are observed to steadily decrease at a somewhat similar rate (Riedo *et al.*, 2013c).

3.2.2. Chemical composition of filaments. The mass spectra of the investigated filaments have a distinctly different chemical composition compared to that of the aragonite host matrix. An example of the mass spectrum of the filament identified at location 36 (M2) is shown in Fig. 6. In the LG spectrum (Fig. 6a), several major (O, Na, Mg, K, Ca, Mn, Fe, and Co) and minor (C, Si, S, Cl) elements are identified. The MG (the channel with a gain intermediate between low and high gain) and HG spectra (6b and 6c)

yield, in addition, the detection of trace elements (B, N, F, Al, P, Ti, Cr, and Ni). Several metallic and nonmetallic elements were readily observed, including (B, N, F, Al, P, S, Cl, Ti, V, Cr, Mn, Fe, Ni, and Co). For most of the elements, the identification is based on the accurate mass determination and the observation of their characteristic isotope pattern. Nevertheless, some of the mass peaks, including N, Si, P, Ti, Fe, Ni, and Co, can coincide with the mass peaks of clusters and molecules, which are expected to form via plasma chemistry in the ablation plume. Particularly troublesome are the carbon molecules and clusters. Carbon is known to be reactive, and it can initiate complex carbon chemistry with production of a variety of carbon molecules and clusters containing H, O, and other elements. Since the mass

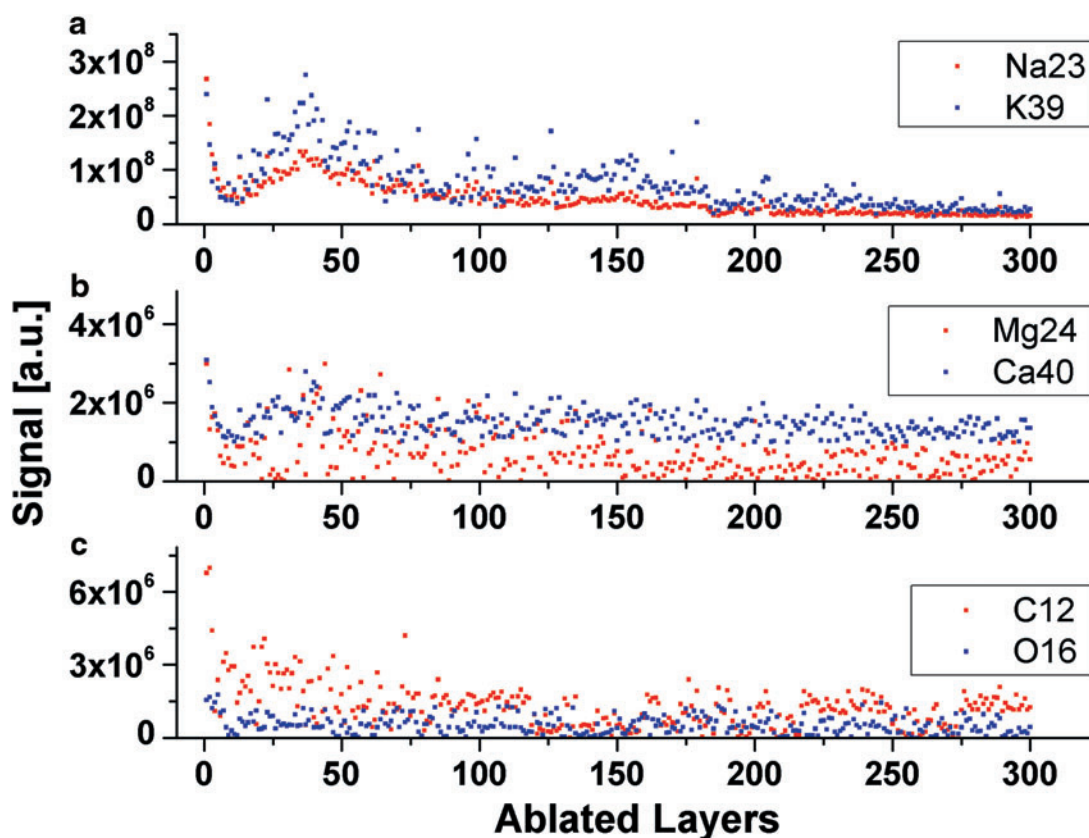


FIG. 5. Chemical depth profiling of the aragonite matrix at location 60 (M2) by means of major elements (see Fig. 2). The changes of the signals of all major elements are observed to be well correlated, and no large variations are observed with the ablation progress. (Color graphics available at www.liebertonline.com/ast)

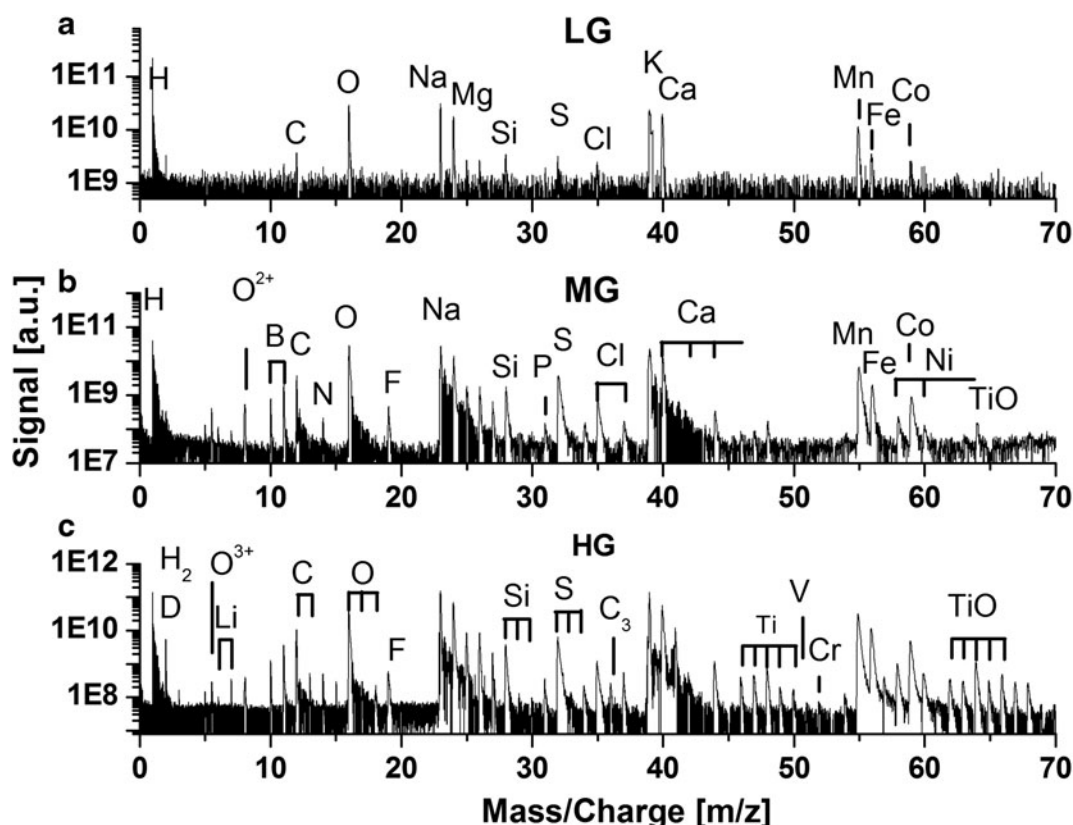


FIG. 6. Typical mass spectrum measured at a filament location. In the LG spectrum (a) the major and minor elements contained in the filament are identified. The medium gain (MG) (b) and HG (c) spectra yield the detection of minor and trace elements as well as clusters and molecules.

spectrometer records mass spectra with a mass resolution of about $m/\Delta m = 400\text{--}600$, the contribution of molecules and clusters to element mass peaks cannot be resolved, and molecules and cluster mass peaks will interfere with mass peaks of elements. The comparison of the mass spectra of aragonite matrix and filaments in the mass ranges of 70–100 also yields a tentative detection of Se, Sr, and Rb. Due to low accuracy of the isotope ratio determination from these spectra, we consider these detections to be tentative.

Figure 7 displays the variation of the element signals with the ablation depth for locations 35 (M2) and 44 (M2) (see also Figs. 2 and 3). By following the S and Mn signal variations with the ablation progress, a sharp transition from the filament to the host matrix can be observed (see Fig. 7). At location 35, the mass spectrometric analysis indicated that the filament was located just below the aragonite surface, and several layers of the aragonite had to be ablated to observe the elements contained only in filaments. In following, weak element signals are observed within 40–75 ablation layers (8000–15,000 laser shots), and subsequently a steady rise of the filament element signals is observed for the next 200 (40,000 laser shots) ablation layers. At location 44, the filament material is observed at the surface level only, within the first 20 ablation layers (4,000 laser shots). In following, weak signals are observed within 25–175 and 200–300 ablation layers. The depth profiling analysis showed that the concentration of elements across ablated layers can be substantially modulated and there are layers at which no filamentous material is observed. In the latter case, only main elements of the aragonite matrix contribute to the spectrum.

While the signal variation of the elements identified in filaments correlates very well with the ablation progress, the relative signals of the main elements (C, O, Mg, Ca, Na, and K) are observed to vary on the transition from the aragonite matrix to filament. The C abundance in the filament is observed to be much lower than that measured in the aragonite matrix, and the O abundance rises in most cases sharply when the studies are conducted on the transition from the aragonite matrix to the filament. Also, the Mg signal is observed to be increasingly larger relative to that of Ca at the filament location. Similarly, the K and Na signals differ in magnitude at the filament location and aragonite matrix, respectively.

Although the differences in the signal magnitudes of C, O, Mg, Ca, Na, K in the filament and matrix for these main elements are readily observed, their atomic fractions cannot be easily determined in the filament material due to limited lateral resolution of these studies. For the filamentous structures smaller than the laser ablation spot, a contribution of the matrix elements to the measured chemical composition would be expected. Table 1 shows an example of the mass spectrometric analysis of filaments by considering a contribution from the main elements only. The analysis takes into account mass spectra measured on a few filaments in both M1 and M2 campaigns. The atomic fractions of relevant elements are observed to not differ substantially between various filaments investigated in both campaigns. They are also similar to the atomic fractions obtained by summing up the spectra of all filaments measured in M1 and M2 campaigns, respectively (see Table 1). The atomic abundance of the main elements—

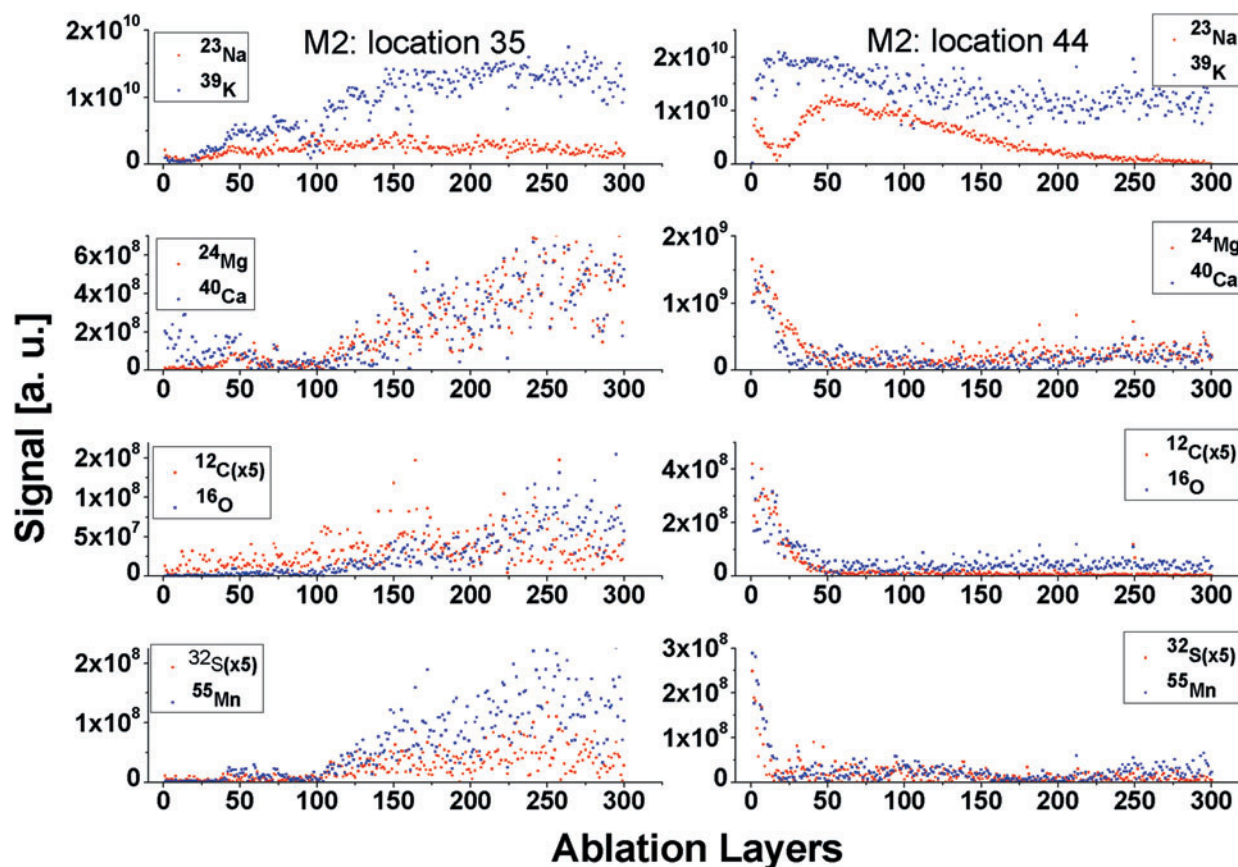


FIG. 7. Depth profiling at surface locations 35 (left panel) and 44 (right panel). At location 35, the filament is reached after ablation of some uppermost layers of aragonite surface. At location 44, most of the filament material is located at the first layers. (Color graphics available at www.liebertonline.com/ast)

Na, K, Ca, and Mg—contained in the filaments differs readily from the abundances in the carbonate phase. For the atomic fractions of Na and K, the analysis yields similar values close to 20%. The mass spectrometric analysis indicates also that the filaments are enriched in Na relative to the carbonate phase. Also, the atomic fraction of Mg is determined to be larger in the filaments than in the carbonate phase and is comparable to the Ca atomic fraction (see Fig. 3 and Table 1). Measurement of the filaments yielded values approximately 14 times lower for the atomic fraction of C compared to O. Typically, the C signal is observed to decrease at the filament, while the O signal rises sharply. This is in contrast to the carbonate phase where a substantially larger atomic fraction of C, as compared with that of O, is measured and the signals are observed to be correlated. All these main elements are also the most abundant in the spectra of filaments, and the atomic fraction of all the other elements contained in the filaments is measured to be in the range of 18–33%.

A number of metallic and nonmetallic elements were measured in the filaments, and their signals were well correlated; the rise and decay of the element signals occur almost with the same rate (Fig. 7). Our studies indicate that these elements are redistributed nearly homogeneously within the filament volume. The instrument has the capability to detect and measure the composition of small mineral grains with sizes down to submicrometer, and if present, they would be identified within the volume of the filament by means of correlation and anti-correlation of elements.

The atomic fractions of elements determined in the filaments are presented in Table 2. The most abundant elements in the investigated filaments are Mn, Fe, Co, Ni, S, Cl, Al, and N. Also Ti, Cr, and V elements were observed occasionally in a few filaments at the trace level.

The results of isotope analysis of the elements contained in filaments are presented in Tables 3 and 4. The studies show that, for most of the major elements, the isotope analysis can be conducted with a few per mill accuracy and precision if signal-to-noise ratio (SNR) is larger than a hundred and there are no isobaric interferences from clusters and molecules that would otherwise affect this ratio (Riedo *et al.*, 2013b, 2013c). For intense mass peaks of C, O, Na, Mg, K, and Ca, there are signal ringing effects observed that can modify mass peak shape and make the peak integration difficult. These are due to a small impedance mismatch and feedback of the ADC components (saturation effect).

The accuracy of isotope ratio determination for the minor and trace elements is readily limited. For the elements identified in the filaments, possible reasons for lack of required accuracy are identified as follows. In the case of the Li isotopes, the ${}^6\text{Li}$ mass peak overlaps with ${}^{12}\text{C}^{+2}$ and the ${}^7\text{Li}$ mass peak with the ${}^{14}\text{N}^{2+}$ mass peak. The mass peak of the carbon isotope ${}^{13}\text{C}$ coincides with the mass peak of the ${}^{12}\text{CH}^{+}$ radical, which can readily form in post-ablation plasma. Similarly, the accuracy of the determination of the O isotopes is affected by the presence of the OH radical in addition to possible ringing effects. Moreover, to investigate

TABLE 2. COMPARISON BETWEEN THE ATOMIC FRACTIONS OF MOST OF THE ELEMENTS DETERMINED FOR FOUR DIFFERENT FILAMENTS AND FOR ALL FILAMENTS INVESTIGATED IN TWO CAMPAIGNS, M1 AND M2, RESPECTIVELY

Element	Location_32 (M1) Fraction [%] ±Abs. error	Location_48 (M1) Fraction [%] ±Abs. error	Total (M1) Fraction [%] ±Abs. error	Location_36 (M2) Fraction [%] ±Abs. error	Location_44 (M2) Fraction [%] ±Abs. error	Total (M2) Fraction [%] ±Abs. error
Li	0.06 (0.01)	0.15 (0.003)	0.31 (0.01)	0.35 (0.01)	0.20 (0.01)	0.15 (0.003)
B	1.77 (0.05)	3.17 (0.02)	2.21 (0.02)	5.00 (0.08)	4.24 (0.05)	2.31 (0.02)
N	1.39 (0.03)	1.06 (0.01)	0.25 (0.01)	0.57 (0.02)	0.39 (0.01)	0.38 (0.002)
F	0.32 (0.02)	0.48 (0.01)	0.53 (0.01)	0.83 (0.02)	0.78 (0.03)	0.38 (0.01)
Si	7.31 (0.08)	6.93 (0.04)	3.43 (0.04)	5.74 (0.05)	5.52 (0.08)	3.43 (0.01)
P	0.25 (0.02)	0.23 (0.01)	0.51 (0.01)	0.60 (0.03)	0.32 (0.02)	0.26 (0.01)
S	3.97 (0.09)	4.26 (0.04)	3.22 (0.04)	14.30 (0.13)	11.37 (0.10)	6.64 (0.02)
Cl	2.60 (0.10)	4.63 (0.04)	3.36 (0.04)	2.07 (0.03)	2.44 (0.05)	2.22 (0.01)
Ti	1.35 (0.07)	0.90 (0.02)	1.32 (0.02)	1.81 (0.03)	1.27 (0.03)	1.73 (0.03)
Mn	49.95 (0.43)	49.79 (0.16)	43.79 (0.16)	36.55 (0.19)	46.90 (0.17)	53.80 (0.03)
Fe	14.60 (0.23)	18.47 (0.10)	27.47 (0.10)	21.83 (0.12)	17.07 (0.09)	21.07 (0.09)
Ni	4.31 (0.08)	2.37 (0.03)	2.11 (0.03)	2.34 (0.04)	1.96 (0.04)	1.19 (0.004)
Co	13.63 (0.13)	12.13 (0.25)	6.97 (0.03)	7.53 (0.05)	8.00 (0.06)	6.27 (0.01)
Li: 460 (60) ppm; V: 60 (50) ppm; Cr: 10 ppm			Li: 300 (50) ppm; V: 260 (5) ppm; Cr: 30 (2) ppm			
N, Al, Cu, Zn: Atomic fraction values are less certain due to isobaric interferences with clusters.			N, Al, Cu, Zn: Atomic fraction values are less certain due to isobaric interferences with clusters.			

the O isotope ratios, large SNR is required. Ringing effects induced by the ^{12}C , ^{23}Na , and ^{39}K signals can affect low intense mass peaks of ^{13}C , ^{24}Mg , and ^{40}Ca , respectively. The presence of carbon clusters formed in postplasma chemistry introduces uncertainty in the analysis of several isotopes (e.g., ^{24}Mg mass peak is more intense due to underlying C_2 cluster). The analysis of heavier elements and their isotopic composition can be affected by more complex

molecules of type $\text{H}_x\text{C}_y\text{O}_z$, which are readily observed in the HG mass spectra obtained either for aragonite host matrix or filaments. Table 3 summarizes the results obtained in the isotope analysis of main elements. In most cases, the analysis of small isotope peaks is limited by SNR of the investigated mass peaks.

The mass peaks of B and S elements are observed to be only somewhat affected by isobaric mass peaks of clusters and

TABLE 3. RESULTS FROM THE ANALYSIS OF THE ISOTOPIC COMPOSITION AND ERROR OF MAJOR ELEMENTS FOR THE FIVE MASS SPECTRA OF THE FILAMENTS; THE FRACTION OF A CERTAIN ISOTOPE, ERROR OF THAT FRACTION (FRACTION ERROR), THE RELATIVE ACCURACY, THE RELATIVE ACCURACY ERROR, AND THE SNR ARE PRESENTED

Location/Isotope		^{16}O	^{18}O	^{39}K	^{41}K	^{40}Ca	^{44}Ca
6_M1	Fraction [%]	99.70	0.16	93.95	6.04	96.94	2.05
	Fraction error	0.78	0.02	0.53	0.03	0.27	0.03
	Heavy isotope accuracy	$\delta^{18}\text{O} = -219$ (110)		$\delta^{41}\text{K} = -11$ (6)		$\delta^{44}\text{Ca} = -17.2$ (8)	
	SNR	2,058	9	8,961	761	3,075	62
32_M1	Fraction [%]	99.71	0.19	93.69	6.30	97.36	1.97
	Fraction error	0.42	0.03	0.47	0.026	0.40	0.03
	Heavy isotope accuracy	$\delta^{18}\text{O} = -73$ (14)		$\delta^{41}\text{K} = -68$ (5)		$\delta^{44}\text{Ca} = +20$ (10)	
	SNR	3,075	23	17,131	1,347	3,812	79
38_M1	Fraction [%]	99.83	0.13	93.87	6.12	97.32	2.0
	Fraction error	0.43	0.01	0.86	0.05	0.26	0.03
	Heavy isotope accuracy	$\delta^{18}\text{O} = -366$ (63)		$\delta^{41}\text{K} = -96$ (11)		$\delta^{44}\text{Ca} = -45$ (9)	
	SNR	1,644	23	4,971	331	855	2,870
44_M2	Fraction [%]	99.53	0.43	93.25	6.74	96.76	2.2
	Fraction error	0.412	0.01	0.49	0.03	0.38	0.02
	Heavy isotope accuracy	$\delta^{18}\text{O} = +1,100$ (160)		$\delta^{41}\text{K} = +1.5$ (3)		$\delta^{44}\text{Ca} = +57$ (11)	
	SNR	2,617	13	23,540	1,865	5,141	109
36_M2	Fraction [%]	99.73	0.23	Spectral quality problem Ringing effects		Spectral quality problem Ringing effects	
	Fraction error	3.89	0.09				
	Heavy isotope accuracy	$\delta^{18}\text{O} = +1122$ (440)					
	SNR	1,000	10				
M2_All	Fraction [%]	99.73	0.22	92.98	7.00	96.86	2.25
	Fraction error	0.91	0.005	4.22	0.23	0.178	0.009
	Heavy isotope accuracy	$\delta^{18}\text{O} = +73$ (43)		$\delta^{41}\text{K} = +43$ (24)		$\delta^{44}\text{Ca} = +79$ (16)	
	SNR	1,400	30	34,500	2,800	1,300	43

TABLE 4. ISOTOPE RATIOS OF THE ELEMENTS B, S, AND CL DETERMINED FOR SEVERAL FILAMENTS DETECTED IN BOTH CAMPAIGNS M1 AND M2, RESPECTIVELY

Isotope		^{10}B	^{11}B	^{32}S	^{34}S	^{35}Cl	^{37}Cl
6_M1	Fraction [%]	23.39	76.61	96.93	2.30	76.35	23.65
	Fraction error	0.41	2.34	0.86	0.13	0.55	0.30
	Heavy isotope accuracy	$\delta^{11}\text{B} [\text{‰}] = -186$ (32)		$\delta^{34}\text{S} [\text{‰}] = -460$ (30)		$\delta^{37}\text{Cl} [\text{‰}] = -31$ (10)	
	SNR	41	60	41	7	170	57
32_M1	Fraction	22.19	77.81	96.19	3.05	76.36	23.6
	Fraction error	1.6	4.2	2.84	0.46	0.73	0.26
	Heavy isotope accuracy	$\delta^{11}\text{B} [\text{‰}] = -129$ (52)		$\delta^{34}\text{S} [\text{‰}] = -286$ (110)		$\delta^{37}\text{Cl} [\text{‰}] = -30$ (11)	
	SNR	11.9	36	46	6	162	44
68_M1	Fraction	23.20	76.80	97.30	2.36	76.00	24.0
	Fraction error	0.34	0.85	0.75	0.006	0.73	0.26
	Heavy isotope accuracy	$\delta^{11}\text{B} [\text{‰}] = -178$ (12)		$\delta^{34}\text{S} [\text{‰}] = -458$ (17)		$\delta^{37}\text{Cl} [\text{‰}] = -12.5$ (4)	
	SNR	44	131	587	20	162	44
36_M2	Fraction	22.17	77.83	96.95	2.54	Underlying cluster peaks	
	Fraction error	0.28	1.3	0.61	0.06		
	Heavy isotope accuracy	$\delta^{11}\text{B} [\text{‰}] = -128$ (22)		$\delta^{34}\text{S} [\text{‰}] = -439$ (29)			
	SNR	71	222	430	20		
44_M2	Fraction	22.03	77.97	97.03	2.66	Underlying cluster peaks	
	Fraction error	0.71	1.79	0.94	0.12		
	Heavy isotope accuracy	$\delta^{11}\text{B} [\text{‰}] = -125$ (15)		$\delta^{34}\text{S} [\text{‰}] = -382$ (38)			
	SNR	21	66	340	10		
M2 total	Fraction	20.92	79.08	96.28	2.94	76.20	23.80
	Fraction error	0.3958	0.6708	0.57	0.07	1.01	0.36
	Heavy isotope accuracy	$\delta^{11}\text{B} [\text{‰}] = -61$ (10)		$\delta^{34}\text{S} [\text{‰}] = -325$ (22)		$\delta^{37}\text{Cl} [\text{‰}] = -22.7$ (7)	

The isotope ratios of B and S are expected to be only little affected by isobaric interference with molecules and clusters, whereas the ^{37}Cl isotope mass peak may interfere with the isobaric C_3H carbon radical.

molecules as well as by detection interferences. The isotope ratio analysis for these two elements was conducted for several filaments identified in both the M1 and M2 campaigns, and the results are presented in Table 4. The results show that the isotope ratios of the lighter isotopes are observed to be larger compared to that measured in the relevant standards. Nevertheless, the accuracy of isotope ratio analysis is too low. One of the main reasons is the low SNR because of a relatively low concentration of S element in filaments. Increasing the number of recorded mass spectra of the filaments helps improve the isotope accuracy to some extent. The results from the analysis of the mass spectra obtained by adding all spectra of filaments measured in M1 and M2, respectively, showed some improvements of the isotope ratio accuracy. More accurate results were obtained for B and Cl for the individual filaments when the mass spectrum obtained by summing up all spectra of filaments was analyzed (Table 4).

4. Discussion

The size and morphology of the observed filaments correspond to known filamentous microorganisms, and their occurrence is similar to fossilized endolithic microorganisms from subseafloor basalts (Ivarsson *et al.*, 2008a, 2008b). Proving biogenicity of putative fossilized microorganisms is a complex task that requires detailed morphological and chemical studies (Ivarsson and Holm, 2006), and it is beyond the scope of this report. The reason we chose these samples was that they were appropriate for the aim of the study. The samples represent the rock type, mafic to ultramafic in composition, that dominates on other planets,

and they contain defined filamentous structures that correspond to the morphology of known fossilized microorganisms in this type of rocks. The aim is thus to develop a methodology with which to analyze such features *in situ*, rather than proving their biogenicity at this stage.

In the present study, we applied chemical mapping and depth profiling methods to isolate filamentous microstructures from the matrix in which they are embedded. This procedure allowed highly accurate spatial localization of the filaments and insight into understanding their shape and element redistribution within the filament volume.

Although no biogenicity can be determined from the current isotope analysis, the elemental composition is suggestive of a biological origin. One also has to consider that diagenetic processes during mineralization may influence the abundances of elements in the putative fossil, and this needs to be accounted for (Castanier *et al.*, 1999; Le Metayer-Levrel *et al.*, 1999). Nevertheless, high abundances of several bio-relevant nonmetallic and metallic elements important in metabolic processes within microbiological systems are found in the filaments but not in the host material (Wackett, 2004a, 2004b, 2004c). High abundances of Mn, Co, Fe, and Ni elements are consistent with their possible accumulation due to life processes (Wackett, 2004b; Ehrlich and Newman, 2008; von Blanckenburg *et al.*, 2008; Cameron *et al.*, 2009). The specific element composition of the filaments is not comparable with the mineralogy of the host rock harzburgite and aragonite; thus the elements have been concentrated into the filaments (Tréhu *et al.*, 2003). Organometallic compounds containing, for example, Mn, Fe, Co, Ni, and Se are important intermediates in the microbial metabolic pathways. Also, biologically common

alkylated elements were determined and include N, S, O, F, and Cl. B is also thought to be important for appropriate biological functionality, but to date its function is poorly understood (Wackett *et al.*, 2004). B can be of environmental interest. The B isotopic fractionation is observed in the environments with hydrous fluids, melts, and minerals where ^{11}B preferentially partitions into the fluid relative to minerals or melts (Liebscher *et al.*, 2005). The most significant mineral on which boron isotope analysis has been conducted, so far, is tourmaline (Meyer *et al.*, 2008; Bast *et al.*, 2014). The lowest observed $\delta^{11}\text{B}$ values are of about -30‰ to -50‰ for certain tourmalines and nonmarine evaporates (Chaussidon and Albarede, 1992; Swihart *et al.*, 1986). The most enriched ^{11}B reservoir is given by brines with $\delta^{11}\text{B}$ values of up to 60‰ (Vengosh *et al.*, 1991). Halogen elements (F, Cl) observed in the filaments can be likely remnants from the salty ocean from which the aragonite mineral was formed. Cl is observed also at trace levels in the aragonite host. Natural isotope variations in Cl isotope ratios are expected due to the mass difference between ^{35}Cl and ^{37}Cl as well as to variations in coordination of Cl in the vapor, aqueous, and solid phases. A natural variation range in Cl isotopic composition is of about 15‰ . In subduction zone pore waters, $\delta^{37}\text{Cl}$ values can be down to 8‰ , and in minerals in which Cl substitutes OH, $\delta^{37}\text{Cl}$ values can reach 7‰ (Ransom *et al.*, 1995). The measurement of S isotopes is an important test of bio-relevant fractionation. Microorganisms are known to fractionate isotopes during sulfur metabolism (dissimilatory sulfate reduction), which produces the largest fractionations in the sulfur cycle. There are also various exchange reactions between sulfate and sulfides that play a role in the isotope differentiation. Wide variations of the $\delta^{34}\text{S}$ values ranging from -65‰ up to 120‰ have been observed (Seal, 2006; Seal *et al.*, 2000). In the present study, isotope fraction analysis conducted for the filaments was not sufficiently accurate to conclude a possible fractionation of B, S, and Cl, though in all cases a light isotope component was determined to be enriched.

While satisfactory results with the isotope ratio accuracy in the range of per mill can be obtained for several elements with SNR values of isotope mass peaks larger than 100, for lower SNR values the isotope ratio accuracy is less accurate (see Tables 3 and 4). This is consistent with the results obtained during the instrument calibration campaigns (Riedo *et al.*, 2013a, 2013b, 2013c). An increase in the instrument sensitivity is possible such that it would compensate for this effect by fine tuning the laser ablation ion source performance (spot size, laser irradiance) and signal amplification. A coupling with a microscope camera system for *on line* visualization of the filaments when performing measurements would be helpful for an accurate overlap of the laser spot on the filament (Tulej *et al.*, 2014).

Taking into account that no special arrangement to the setup was made during measurement of micrometer-structures, the obtained results are encouraging. Mass spectrometric investigation of micrometer-sized particles is generally difficult, and typically only advanced laboratory instrumentation can deliver relevant chemical information (Zinner *et al.*, 2011). Our investigation proves high sensitivity in the measurement of elements and isotope ratios. To improve the accuracy of the latter, the sensitivity of measurements has to be increased when such small objects are a subject of investigation.

5. Summary

Analysis of the chemical composition of micrometer-sized filamentous structures embedded in an aragonite host mineral were performed with a laser ablation/ionization mass spectrometer designed for *in situ* space research. Analyses yielded the element composition of the host material and filaments. The major elements detected in the aragonite mineral were H, C, O, Na, Mg, K, and Ca; and two trace elements, S and Cl, were measured at the few-parts-per-million level. The investigated filaments contain distinct atomic fractions of nonmetallic (Li, B, N, F, P, and S) and metallic (Mn, Fe, Co, Ni) elements in addition to elements that were also detected in the aragonite matrix. It will be more difficult to derive fractions of Ca, Mg, C, and O at the present time because of a possible contribution from the aragonite matrix. Nevertheless, substantial differences between the abundances of these elements in filaments and the aragonite matrix were observed. Traces of Ti, V, Cr, Se, and Sr were also observed, but their atomic fractions could not be determined with high accuracy due to isobaric interferences. The detection of high atomic fractions of bio-relevant elements, including B, S, Mn, Co, Fe, and Se, is considered to be in favor of a bio-origin of the investigated filaments. Enrichment of the light isotope of S was measured for all investigated filaments, but the accuracy of the measurement is presently too low. A few other abundant elements, including B, F, and Cl, were observed in filaments. These can be important in metabolic processes, but they can also be remnants of the ocean where the aragonite mineral was formed. The present study forms the basis for further investigation of these putative fossils by other analytical instrumentation. The laser ablation/ionization mass spectrometer has proved to be highly sensitive and allow for high spatial resolution to deliver sensitive measurements of the element composition of microstructures. Although at present the isotope analysis is not sufficiently accurate, improvements of these measurements can be made by optimizing the laser ablation ion source conditions and instrument sensitivity with the intent to increase the SNR of the detected isotopes. By combining LMS with a microscope-camera system, direct viewing of microstructures will be helpful in optimizing measurement efficiency. Such a suite would also be of considerable interest for *in situ* investigation of planetary surfaces.

Acknowledgments

This work was supported by the Swiss National Science Foundation Grant No. 200020_153047. We wish to acknowledge Wolfgang Bach at Bremen University for providing the samples. M. Ivarsson is funded by the Swedish Research Council (Contract No. 2012-4364) and Danish National Research Foundation (DNRF53). A. Neubeck is funded by the Swedish National Space Board (Dnr: 100/13) and the Royal Swedish Academy of Sciences.

Author Disclosure Statement

No competing financial interests exist.

References

- Bach, W., Rosner, M., Jons, N., Rausch, S., Robinson, L.F., Paulick, H., and Erzinger, J. (2011) Carbonate veins trace

- seawater circulation during exhumation and uplift of mantle rock: results from ODP Leg 209. *Earth Planet Sci Lett* 311:242–252.
- Bast, R., Scherer, E.E., Mezger, K., Austrheim, H., Ludwig, T., Marschall, H.R., Putnis, A., and Lowen, K. (2014) Boron isotopes in tourmaline as a tracer of metasomatic processes in the Bamble sector of Southern Norway. *Contrib Mineral Petrol* 168:1069.
- Bishop, J.L., Dobrea, E.Z.N., McKeown, N.K., Parente, M., Ehlmann, B.L., Michalski, J.R., Milliken, R.E., Poulet, F., Swayze, G.A., Mustard, J.F., Murchie, S.L., and Bibring, J.P. (2008) Phyllosilicate diversity and past aqueous activity revealed at Mawrth Vallis, Mars. *Science* 321:830–833.
- Brasier, M.D., Green, O.R., Lindsay, J.F., McLoughlin, N., Steele, A., and Stoakes, C. (2005) Critical testing of Earth's oldest putative fossil assemblage from the similar to 3.5 Ga Apex Chert, Chinaman Creek, Western Australia. *Precambrian Res* 140:55–102.
- Brinckerhoff, W.B., Managadze, G.G., McEntire, R.W., Cheng, A.F., and Green, W.J. (2000) Laser time-of-flight mass spectrometry for space. *Rev Sci Instrum* 71:536–545.
- Cameron, V., Vance, D., Archer, C., and House, C.H. (2009) A biomarker based on the stable isotopes of nickel. *Proc Natl Acad Sci USA* 106:10944–10948.
- Castanier, S., Le Metayer-Levrel, G., and Perthuisot, J.P. (1999) Ca-carbonates precipitation and limestone genesis—the microbiogeologist point of view. *Sediment Geol* 126:9–23.
- Chaussidon, M. and Albarede, F. (1992) Secular boron isotope variations in the continental-crust—an ion microprobe study. *Earth Planet Sci Lett* 108:229–241.
- Chela-Flores, J. (2010) Instrumentation for the search for habitable ecosystems in the future exploration of Europa and Ganymede. *International Journal of Astrobiology* 9:101–108.
- Chela-Flores, J. (2012) A case for landing on the Moon's far-side to test nitrogen abundances. *International Journal of Astrobiology* 11:61–69.
- Chela-Flores, J. and Kumar, N. (2008) Returning to Europa: can traces of surficial life be detected? *International Journal of Astrobiology* 7:263–269.
- Chela-Flores, J. and Seckbach, J. (2011) The Dry Valley Lakes, Antarctica: from sulfur stains on Earth to sulfur stains in the jovian system. *Proc SPIE* 8152, doi:10.1117/12.898763.
- Chela-Flores, J., Cicuttin, A., Crespo, M.L., and Tuniz, C. (2015) Biogeochemical fingerprints of life: earlier analogies with polar ecosystems suggest feasible instrumentation for probing the Galilean moons. *International Journal of Astrobiology* 14:427–434.
- Ehrlich, H.L. and Newman, D.K. (2008) *Geomicrobiology*, CRC Press, Boca Raton, FL.
- Farmer, J.D. (2001) Hydrothermal systems on Mars: an assessment of present evidence. In *Evolution of Hydrothermal Ecosystems on Earth (and Mars?)*, Ciba Foundation Symposium 202, edited by G.R. Bock and J.A. Goode, Wiley and Sons, Chichester, UK, pp 273–303.
- Gorbushina, A. (2003) Microcolonial fungi: survival potential of terrestrial vegetative structures. *Astrobiology* 3:543–554.
- Gorbushina, A.A., Krumbein, W.E., and Volkmann, M. (2002) Rock surfaces as life indicators: new ways to demonstrate life and traces of former life. *Astrobiology* 2:203–213.
- Grimaud, V., Moreno-Garcia, P., Riedo, A., Neuland, M.B., Tulej, M., Broekmann, P., and Wurz, P. (2015) High-resolution chemical depth profiling of solid material using a miniature laser ablation/ionization mass spectrometer. *Anal Chem* 87:2037–2041.
- Grotzinger, J.P., Crisp, J., Vasavada, A.R., Anderson, R.C., Baker, C.J., Barry, R., Blake, D.F., Conrad, P., Edgett, K.S., Ferdowski, B., Gellert, R., Gilbert, J.B., Golombek, M., Gómez-Elvira, J., Hassler, D.M., Jandura, L., Litvak, M., Mahaffy, P., Maki, J., Meyer, M., Malin, M.C., Mitrofanov, I., Simmonds, J.J., Vaniman, D., Welch, R.V., and Wiens, R.C. (2012) Mars Science Laboratory mission and science investigation. *Space Sci Rev* 170:5–56.
- Ireland, T.R. (2013) Invited review article: recent developments in isotope-ratio mass spectrometry for geochemistry and cosmochemistry. *Rev Sci Instrum* 84, doi:10.1063/1.4765055.
- Ivarsson, M. and Holm, N.G. (2006) Mn as a potential energy source for seafloor chemoautotrophs. *Geochim Cosmochim Acta* 70:A282.
- Ivarsson, M., Lausmaa, J., Lindblom, S., Broman, C., and Holm, N.G. (2008a) Fossilized microorganisms from the Emperor Seamounts: implications for the search for a subsurface fossil record on Earth and Mars. *Astrobiology* 8:1139–1157.
- Ivarsson, M., Lindblom, S., Broman, C., and Holm, N.G. (2008b) Fossilized microorganisms associated with zeolite-carbonate interfaces in sub-seafloor hydrothermal environments. *Geobiology* 6:155–170.
- Le Metayer-Levrel, G., Castanier, S., Orial, G., Loubiere, J.F., and Perthuisot, J.P. (1999) Applications of bacterial carbonatogenesis to the protection and regeneration of limestones in buildings and historic patrimony. *Sediment Geol* 126:25–34.
- Leshin, L.A., Mahaffy, P.R., Webster, C.R., Cabane, M., Coll, P., Conrad, P.G., Archer, P.D., Atreya, S.K., Brunner, A.E., Buch, A., Eigenbrode, J.L., Flesch, G.J., Franz, H.B., Freissinet, C., Glavin, D.P., McAdam, A.C., Miller, K.E., Ming, D.W., Morris, R.V., Navarro-González, R., Niles, P.B., Owen, T., Pepin, R.O., Squyres, S., Steele, A., Stern, J.C., Summons, R.E., Sumner, D.Y., Sutter, B., Szopa, C., Teinturier, S., Trainer, M.G., Wray, J.J., Grotzinger, J.P.; the MSL Science Team. (2013) Volatile, isotope, and organic analysis of martian fines with the Mars Curiosity rover. *Science* 341, doi:10.1126/science.1238937.
- Liebscher, A., Meixner, A., Romer, R.L., and Heinrich, W. (2005) Liquid-vapor fractionation of boron and boron isotopes: experimental calibration at 400 degrees C/23 MPa to 450 degrees C/42 MPa. *Geochim Cosmochim Acta* 69:5693–5704.
- Managadze, G.G., Wurz, P., Sagdeev, R.Z., Chumikov, A.E., Tuley, M., Yakovleva, M., Managadze, N.G., and Bondarenko, A.L. (2010) Study of the main geochemical characteristics of Phobos' regolith using laser time-of-flight mass spectrometry. *Solar System Research* 44:376–384.
- Meyer, C., Wunder, B., Meixner, A., Romer, R.L., and Heinrich, W. (2008) Boron-isotope fractionation between tourmaline and fluid: an experimental re-investigation. *Contrib Mineral Petrol* 156:259–267.
- Mustard, J.F., Murchie, S.L., Pelkey, S.M., Ehlmann, B.L., Milliken, R.E., Grant, J.A., Bibring, J.P., Poulet, F., Bishop, J., Dobrea, E.N., Roach, L., Seelos, F., Arvidson, R.E., Wiseman, S., Green, R., Hash, C., Humm, D., Malaret, E., McGovern, J.A., Seelos, K., Clancy, T., Clark, R., Des Marais, D., Izenberg, N., Knudson, A., Langevin, Y., Martin, T., McGuire, P., Morris, R., Robinson, M., Roush, T., Smith, M., Swayze, G., Taylor, H., Titus, T., and Wolff, M. (2008) Hydrated silicate minerals on Mars observed by the Mars Reconnaissance Orbiter CRISM instrument. *Nature* 454:305–309.
- Neuland, M.B., Meyer, S., Mezger, K., Riedo, A., Tulej, M., and Wurz, P. (2014) Probing the Allende meteorite with a miniature laser-ablation mass analyser for space application. *Planet Space Sci* 101:196–209.

- Parnell, J., Cullen, D., Sims, M.R., Bowden, S., Cockell, C.S., Court, R., Ehrenfreund, P., Gaubert, F., Grant, W., Parro, V., Rohmer, M., Sephton, M., Stan-Lotter, H., Steele, A., Toporski, J., and Vago, J. (2007) Searching for life on Mars: selection of molecular targets for ESA's Aurora ExoMars mission. *Astrobiology* 7:578–604.
- Ransom, B., Spivack, A.J., and Kastner, M. (1995) Stable Cl Isotopes in subduction-zone pore waters—implications for fluid-rock reactions and the cycling of chlorine. *Geology* 23:715–718.
- Reysenbach, A.L. and Cady, S.L. (2001) Microbiology of ancient and modern hydrothermal systems. *Trends Microbiol* 9:79–86.
- Riedo, A. (2014) Development and performance evaluation of a laser ablation ionisation mass spectrometer for *in situ* planetary exploration. PhD thesis, University of Bern, Bern, Switzerland.
- Riedo, A., Wahlstrom, P., Scheer, J.A., Wurz, P., and Tulej, M. (2010) Effect of long-duration UV irradiation on diamondlike carbon surfaces in the presence of a hydrocarbon gaseous atmosphere. *J Appl Phys* 108:1–15.
- Riedo, A., Bieler, A., Neuland, M., Tulej, M., and Wurz, P. (2013a) Performance evaluation of a miniature laser ablation time-of-flight mass spectrometer designed for *in situ* investigations in planetary space research. *J Mass Spectrom* 48:1–15.
- Riedo, A., Meyer, S., Heredia, B., Neuland, M.B., Bieler, A., Tulej, M., Leya, I., Iakovleva, M., Mezger, K., and Wurz, P. (2013b) Highly accurate isotope composition measurements by a miniature laser ablation mass spectrometer designed for *in situ* investigations on planetary surfaces. *Planet Space Sci* 87:1–13.
- Riedo, A., Neuland, M., Meyer, S., Tulej, M., and Wurz, P. (2013c) Coupling of LMS with a fs-laser ablation ion source: elemental and isotope composition measurements. *J Anal At Spectrom* 28:1256–1269.
- Rohner, U., Whitby, J.A., and Wurz, P. (2003) A miniature laser ablation time-of-flight mass spectrometer for *in situ* planetary exploration. *Meas Sci Technol* 14:2159–2164.
- Rohner, U., Whitby, J.A., Wurz, P., and Barabash, S. (2004) Highly miniaturized laser ablation time-of-flight mass spectrometer for a planetary rover. *Rev Sci Instrum* 75:1314–1322.
- Seal, R.R. (2006) Sulfur isotope geochemistry of sulfide minerals. *Sulfide Mineralogy and Geochemistry* 61:633–677.
- Seal, R.R., Alpers C.N., and Rye, R.O. (2000) Stable isotope systematics of sulfate minerals. *Sulfate Minerals—Crystallography, Geochemistry and Environmental Significance* 40:541–602.
- Squyres, S.W., Arvidson, R.E., Ruff, S., Gellert, R., Morris, R.V., Ming, D.W., Crumpler, L., Farmer, J.D., Des Marais, D.J., Yen, A., McLennan, S.M., Calvin, W., Bell, J.F., III, Clark, B.C., Wang, A., McCoy, T.J., Schmidt, M.E., and de Souza, P.A., Jr. (2008) Detection of silica-rich deposits on Mars. *Science* 320:1063–1067.
- Summons, R.E., Amend, J.P., Bish, D., Buick, R., Cody, G.D., Des Marais, D.J., Dromart, G., Eigenbrode, J.L., Knoll, A.H., and Sumner, D.Y. (2011) Preservation of martian organic and environmental records: final report of the Mars Biosignature Working Group. *Astrobiology* 11:157–181.
- Swihart, G.H., Moore, B., and Callis, E.L. (1986) Boron isotopic composition of marine and nonmarine evaporite borates. *Geochim Cosmochim Acta* 50:1297–1301.
- Tréhu, A.M., Bohrmann, G., Rack, F.R., Torres, M.E., Bangs, N.L., Barr, S.R., Borowski, W.S., Claypool, G.E., Collett, T.S., Delwiche, M.E., Dickens, G.R., Goldberg, D.S., Gràcia, E., Guérin, G., Holland, M., Johnson, J.E., Lee, Y.-J., Liu, C.-S., Long, P.E., Milkov, A.V., Riedel, M., Schultheiss, P., Su, X., Teichert, B., Tomaru, H., Vanneste, M., Watanabe, M., and Weinberger, J.L. (2003) *Proceedings of the Ocean Drilling Program*, Vol. 204 Initial Reports, Ocean Drilling Program, College Station, TX.
- Tulej, M., Iakovleva, M., Leya, I., and Wurz, P. (2011) A miniature mass analyser for *in situ* elemental analysis of planetary material—performance studies. *Anal Bioanal Chem* 399:2185–2200.
- Tulej, M., Riedo, A., Neuland, M.B., Meyer, S., Wurz, P., Thomas, N., Grimaudo, V., Moreno-Garcia, P., Broekmann, P., Neubeck, A., and Ivarsson, M. (2014) CAMAM: a miniature laser ablation ionisation mass spectrometer and microscope-camera system for *in situ* investigation of the composition and morphology of extraterrestrial materials. *Geostandards and Geoanalytical Research* 38:441–466.
- Vengosh, A., Kolodny, Y., Starinsky, A., Chivas, A.R., and McCulloch, M.T. (1991) Coprecipitation and isotopic fractionation of boron in modern biogenic carbonates. *Geochim Cosmochim Acta* 55:2901–2910.
- von Blanckenburg, F., Marnberti, M., Schoenberg, R., Kamber, B.S., and Webb, G.E. (2008) The iron isotope composition of microbial carbonate. *Chem Geol* 249:113–128.
- Wackett, L.P. (2004a) Evolution of enzymes for the metabolism of new chemical inputs into the environment. *J Biol Chem* 279:41259–41262.
- Wackett, L.P. (2004b) Novel biocatalysis by database mining. *Curr Opin Biotechnol* 15:280–284.
- Wackett, L.P. (2004c) Stable isotope probing in biodegradation research. *Trends Biotechnol* 22:153–154.
- Wackett, L.P., Dodge, A.G., and Ellis, L.B.M. (2004) Microbial genomics and the periodic table. *Appl Environ Microbiol* 70:647–655.
- Westall, F., Nijman, W., Brack, A., Steele, A., and Toporski, J. (2001) The oldest fossil life on Earth, its geological context and life on Mars. In *Exo-/Astro-Biology: Proceedings of the First European Workshop*, ESA SP-496, edited by P. Ehrenfreund, O. Angerer, and B. Battrick, ESA Publications Division, Noordwijk, the Netherlands, pp 81–90.
- Zinner, E.K., Moynier, F., and Stroud, R.M. (2011) Laboratory technology and cosmochemistry. *Proc Natl Acad Sci USA* 108:19135–19141.

Address correspondence to:
Marek Tulej
Physics Institute
University of Bern
Sidlerstrasse 5
CH-3012 Bern
Switzerland

E-mail: marek.tulej@space.unibe.ch

Submitted 15 February 2015

Accepted 15 June 2015

Abbreviations Used

EDS = energy-dispersive spectrometer
ESEM = environmental scanning electron microscope
HG = high gain
LG = low gain
LMS = laser ablation/ionization time-of-flight mass spectrometer
MG = medium gain
SNR = signal-to-noise ratio